

# Phase diagram and magnetic properties of $\text{La}_{1-x}\text{Ca}_x\text{MnO}_3$ compound for $0 \leq x \leq 0.23$ .

M. Pissas and G. Papavassiliou

*Institute of Materials Science, NCSR, Demokritos, 153 10 Aghia Paraskevi, Athens, Greece*

(Dated: May 21, 2021)

In this article a detailed study of  $\text{La}_{1-x}\text{Ca}_x\text{MnO}_3$  ( $0 \leq x \leq 0.23$ ) phase diagram using powder x-ray diffraction and magnetization measurements is presented. Unfortunately, in the related literature no properly characterized samples have been used, with consequence the smearing of the real physics in this complicated system. As the present results reveal, there are two families of samples. The first family concerns samples prepared in atmosphere ( $P(\text{O}_2) = 0.2 \text{ Atm}$ ) which are all ferromagnetic with Curie temperature rising with  $x$ . The second family concerns samples, where a post annealing in nearly zero oxygen partial pressure is applied. These samples show a canted antiferromagnetic structure for  $0 \leq x \leq 0.1$  below  $T_N$ , while for  $0.125 \leq x < 0.23$  an unconventional ferromagnetic insulated phase is present below  $T_c$ . The most important difference between nonstoichiometric and stoichiometric samples concerning the magnetic behavior, is the anisotropy in the exchange interactions, in the stoichiometric samples putting forward the idea that a new orbital ordered phase is responsible for the ferromagnetic insulating regime in the  $\text{La}_{1-x}\text{Ca}_x\text{MnO}_3$  compound.

PACS numbers: 74.60.Ge, 74.60.Jg, 74.60.-w, 74.62.Bf

## I. INTRODUCTION

Manganite perovskites  $\text{RE}_{1-x}\text{AR}_x\text{MnO}_3$  (RE=La and rear earths, AR=Ca, Sr, Ba) display interesting and puzzling structural, magnetic and transport properties. The reason for this is the close interplay between charge, spin and lattice degrees of freedom. One of the most popular detailed studied system, concerning the transport, structural, and magnetic properties<sup>1,2,3,4,5,6,7,8</sup> is the Ca-based  $\text{La}_{1-x}\text{Ca}_x\text{MnO}_3$  ( $0 \leq x \leq 1$ ) compound. In stoichiometric  $\text{LaMnO}_3$  at  $T_{\text{RO}}$ , a structural rhombohedral (R) to orthorhombic (O) transition occurs. In the O phase the  $\text{MnO}_6$  octahedra attempt specific tilting system due to the particular value of the tolerance factor. Mn ions in an undistorted octahedral oxygen coordination have an electronic structure  $d^4 = t_{2g}^3 e_g^1$  (one electron on a doubly degenerated  $e_g$ -orbital). Subsequently at  $T_{\text{JT}}$   $\text{LaMnO}_3$  is transformed from O to another orthorhombic structure (O'). In the O phase the three octahedral MnO bond lengths are almost equal. The transition at  $T_{\text{JT}}$  originates from a cooperative Jahn-Teller structural transition<sup>9,11</sup> resulting in to anisotropic Mn-O bond lengths, with the long bond ordered in a two sublattice fashion<sup>10</sup> in the  $ac$  plane. This particular ordering of the long bonds in the basal  $ac$ -plane ( $Pnma$  notation) has been connected with the orbital ordering of the  $d_{x^2}$  and  $d_{z^2}$  orbitals. Finally, at  $T_N$  the compound is ordered antiferromagnetically attempting the so-called antiferromagnetic structure ( $\mathbf{m}||a$ -axis) ferromagnetic layers coupled antiferromagnetically along  $b$ -axis). Such an ordering is connected with the orbital ordering. The antiferromagnetic interactions along  $b$ -axis have to do with the three  $t_{2g}$  electrons. The strong overlap between half filled orbitals  $d_{x^2}$  at site 1 and an empty one  $d_{x^2-y^2}$  at site 2 gives the ferromagnetic exchange<sup>11</sup> (at  $ac$ -plane, in accordance with the Goodenough-Kanamori-Anderson rules).

The substitution of La by Ca, i.e. doping the compound with holelike charge carriers, induces drastic

changes of the structural and magnetic/transport properties. In the doping level  $0.0 < x \leq 0.1$  the long magnetically ordered state for  $T < T_c$  is a canted antiferromagnetic structure (CAF) closely connected with the A-antiferromagnetic structure of  $\text{LaMnO}_3$  compound, where the collinear magnetic moments in the  $ac$ -plane, are canted in such a way producing a net ferromagnetic component along  $b$ -axis<sup>12</sup>. The anisotropy of the Mn-O bond lengths in the O' phase are still present, with a tendency for reduction as  $x$  increases. Based on the assumption that this ordering of the long bonds is connected with the orbital ordering, the orbital ordering is preserved, also in the CAF regime.

With further doping  $0.125 < x < 0.23$  the CAF phase is transformed to a ferromagnetic insulating phase in contradiction with the conventional double and superexchange models. to 80 K this phase follows the O' structure<sup>13</sup> with moderate anisotropic Mn-O bond lengths. As the doping concentration  $x$  increases, the static JT distortion weakens progressively and the system becomes metallic and ferromagnetic for  $x > 0.23$ . It is believed that in the absence of a cooperative effect in this regime, local JT distortions persist<sup>14,15,16</sup> on short time and length scales. These short-range correlations, together with the electron correlations, would create the effective carrier mass necessary for large magnetoresistance.

The ferromagnetic insulating phase is one of the most puzzling regime in the physics of manganites perovskites. Several models have been proposed to interpret it especially for the  $\text{La}_{1-x}\text{Sr}_x\text{MnO}_3$  compound, including new orbital and charge ordering<sup>17,18</sup> states. Although, a lot of experimental studies have been devoted for the ferromagnetic insulating regime of the  $\text{La}_{1-x}\text{Ca}_x\text{MnO}_3$  compound, in most of them, significantly nonstoichiometric samples were used, leading, (as it is pointed out by Dabrowski et al. Ref.<sup>19</sup>) in contradictory results if one compares results of different groups. The nonstoichio-

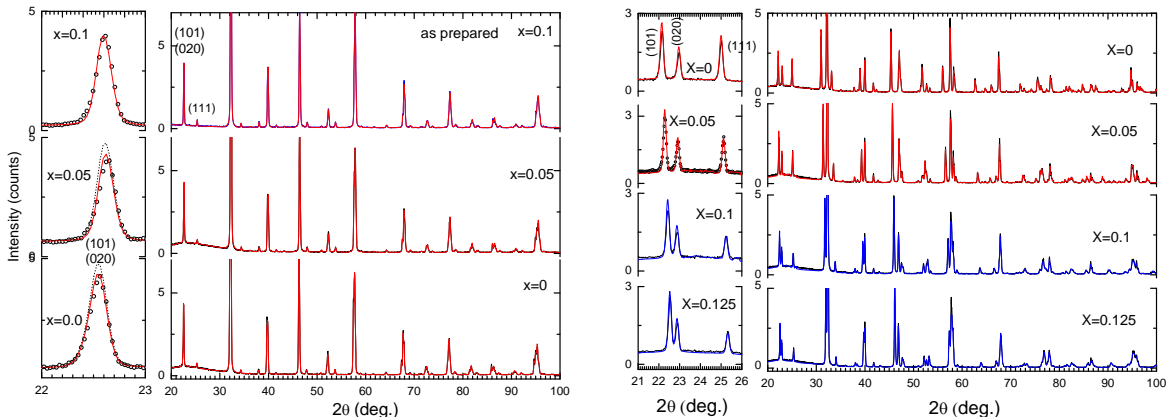


FIG. 1: XRD patterns of as prepared in air atmosphere at  $1400^\circ$  (a) and post annealed at  $1000^\circ\text{C}$  in high purity He  $\text{La}_{1-x}\text{Ca}_x\text{MnO}_3$  samples (b). At the left of the main panel is a magnification of the patterns near the (101), (020) reflections.

metric samples although showing ferromagnetic insulating behavior for  $x < 0.2$ , most probably concern samples with cation vacancies where the unknown orbital state of the ferromagnetic insulating regime, is probably in a liquid state. In addition, the concentration gradients in the single crystals (when they are free of vacancies) make difficult the direct comparison of the results between different composition and research groups. The main reason for this is the fact that the crystal chemistry and physical properties of the low Ca-samples depend on the partial pressure of the oxygen during the sample preparation. As the results of the present study reveal, there are two families of samples. The first family concerns samples prepared in air atmosphere ( $P(\text{O}_2) = 0.2 \text{ Atm}$ ) displaying ferromagnetic behavior with Curie temperature which diminishes as  $x$  goes to zero. The second family concerns samples where a post annealing in nearly zero oxygen partial pressure is applied, leading to a complicated phase diagram. A first attempt in understanding how the preparation conditions influence the phase diagram of  $\text{La}_{1-x}\text{Ca}_x\text{MnO}_3$  ( $0 \leq x \leq 0.2$ ) has been performed by Dabrowski et al. and Huang et al., in Refs.<sup>19,20,21</sup>. In these studies the role of the oxygen partial pressure has been recognized as the key parameter influencing the  $\text{Mn}^{+4}$  amount, in addition to the nominal calcium content. Taking into account these observations one must be cautious in adopting theoretical models before the basic solid state chemistry and the complete characterization of the  $\text{La}_{1-x}\text{Ca}_x\text{MnO}_3$  compound is made.

In the present paper we carry out a detailed study in respect of bulk magnetic properties of  $\text{La}_{1-x}\text{Ca}_x\text{MnO}_3$  ( $0 \leq x \leq 0.23$ ) in two sets of samples, in an effort, firstly to elucidate the complications that originate from the nonstoichiometry of the samples and secondly, using magnetic and resistivity measurements, to understand the differences in magnetic properties between the two families of compounds.

## II. EXPERIMENTAL DETAILS

$\text{La}_{1-x}\text{Ca}_x\text{MnO}_3$  samples were prepared by thoroughly mixing stoichiometric amounts preheated  $\text{La}_2\text{O}_3$ ,  $\text{CaCO}_3$  and  $\text{MnO}_2$  following a solid-state reaction method, in air at  $1400^\circ\text{C}$ . We call these samples "air prepared" (AP). Part of the AP samples was subsequently post annealed at  $1000^\circ\text{C}$  in high purity He flow. These samples are called reduced samples (R). X-ray powder diffraction (XRD) data were collected with a D500 SIEMENS diffractometer, using  $\text{CuK}\alpha$  radiation. The Rietveld refinement of the XRD data is performed by using the FULLPROF program.<sup>22</sup> DC magnetization measurements were performed in a superconducting quantum interference device (SQUID) magnetometer (Quantum Design MPMS2). For ac susceptibility measurements a home made susceptometer was employed. The dc, the drive and pickup coils are inside the cryogenic fluid, in order to have measurements in a constant background.

## III. X-RAY DIFFRACTION DATA

Figure 1 shows part of the XRD patterns of the AP and R samples. Based on Rietveld method both set of samples can structurally be described by using the  $Pnma$  space group. In addition, the R samples display the cooperative Jahn-Teller structure, which is characterized by the splitting of (101) and (020) diffraction peaks. As the Rietveld refinement revealed, in each  $\text{MnO}_6$  octahedron there are three different bonds, with the medium length Mn-O<sub>1</sub> bond (m) directed along the b-axis and the long (l) and short (s) Mn-O<sub>2</sub> bonds alternating along the  $a$  and  $c$  axes ( $Pnma$  notation).

Despite the fact that XRD data of all AP-samples are indicative for single phase samples, all the samples (see below) are ferromagnetic. No cooperative Jahn-Teller distortion is present for the AP samples as the

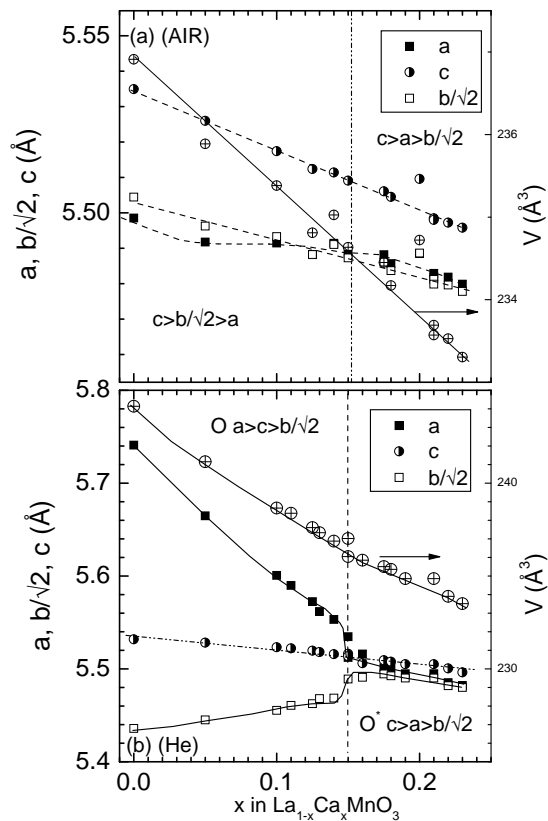


FIG. 2: (a) Concentrations dependence of unit cell constants and volume for (AP) (a) and (R) (b)  $\text{La}_{1-x}\text{Ca}_x\text{MnO}_3$  samples.

unit cell constants and the Mn-O bond-lengths point out, even for samples with  $x < 0.1$ . *Most probably, all these AP-samples concern cation deficient samples.* One may claim that the oxygen content for this family of samples, is larger than for the stoichiometric ones. However, the  $\text{LaMnO}_3$  perovskite-type structure is a closed-packed  $\text{LaO}_3$  lattice with Mn ions in the octahedral sites completely surrounded by oxygens ions. The possible sites for interstitial ions (tetrahedral and octahedral) are surrounded by negatively charged ions (oxygens) as well as by positively charged ions (lanthanum). It is very hard to incorporate charged particles into these sites. Consequently, a cation vacancies<sup>20</sup> structure can explain the variation of the crystal-chemistry and the physical properties of  $\text{La}_{1-x}\text{Ca}_x\text{MnO}_3$  system for  $0 \leq x \leq 0.23$ . Most importantly, refining the atomic positional and isotropic thermal parameters, keeping the occupancy factors according to the nominal composition, did not yield a completely satisfactory refinement because some peaks (e.g. (101), (020)) did not have the adequate intensity. Including as additional free parameters the occupation factors for La and Mn, a clear improvement of the fit was achieved, and moreover these peaks got the right intensity. The results of the refinement clearly show that a nearly equal amount of La and Mn vacancies are present

in the AP samples. The La and Mn deficiency decreases as  $x$  increases.

Figure 2 shows the concentration variation of the unit cell parameters for AP and R samples. While for the AP samples the cell constants are reduced monotonically as  $x$  increases, the corresponding variation of the R samples show a clear change in the slope at around  $x \approx 0.15$ . For higher  $x$  there is not substantial difference between the variation of the cell constants of the AP and R samples. It is interesting to be noted that the unit-cell volume changes monotonously with  $x$  as is expected from the smaller ionic radius both of the  $\text{Ca}^{+2}$  and  $\text{Mn}^{+4}$ . However, the slope differ by a factor of two in the two families of samples, e.g.  $(d(V/V_0)/dx) = -0.1455$  for AP samples and  $(d(V/V_0)/dx) = -0.27$ , for the R samples ( $V_0$  is the unit cell volume at  $x = 0$  for AP and R samples respectively). The difference in the unit-cell reduction slope most probably is related with the cooperative Jahn-Teller distortion, which is present only in the R samples. The abrupt changes of the unit-cell parameters for  $x < 0.15$  is the result of the intersection of the Jahn-Teller transition curve (e.g for  $x < 0.15$ ,  $T_{JT}(x) > 300$  K). Both families of samples exhibit a  $\text{GdFeO}_3$  distortion of the perovskite structure. Orthorhombic perovskites have been separated into type  $O^*$  ( $b/c > \sqrt{2}$ ,  $Pnma$  notation), wherein the predominant distortion is octahedral tilting as in  $\text{GdFeO}_3$  and type  $O^-$  ( $b/c < \sqrt{2}$ , wherein the predominant distortion is driven by the cooperative Jahn-Teller effect. The R samples at  $T = 300$  K up to  $x = 0.15$  are described by the  $O^-$ -structure. We must note that the difficulty in preparing homogenous samples in the  $x = 0.15$  regime is related with the fact that the cooperative JT distortion, at the particular concentration, occurs near  $T = 300$  K.

#### IV. MAGNETIC MEASUREMENTS

Proceeding further we carry out both dc- magnetic moment and ac-susceptibility measurements in order to estimate the magnetic phase diagram of the two families of samples. Figure 3 shows the temperature dependence of the magnetic moment for both AP and R  $\text{LaMnO}_3$  samples. The AP sample shows a paramagnetic to ferromagnetic transition at  $T_c = 165$  K. The temperature variation of the magnetic moment shows strong hysteretic behavior depending on the measuring mode. In zero field cooling mode (ZFC) the moment initially increases slightly up to 80 K. In a relatively narrow temperature interval a step-like increasing of the magnetic moment is observed. We characterize this feature by its onset temperature, during cooling, denoted by  $T_B$ . Subsequently the moment increases up to 150 K and then sharply decreases at Curie temperature. The width of the transition at  $T_c$  is relatively sharp in comparison with ferromagnetic-paramagnetic transitions observed in higher concentrations. This sharp decreasing of the magnetic moment may be implying a first order magnetic

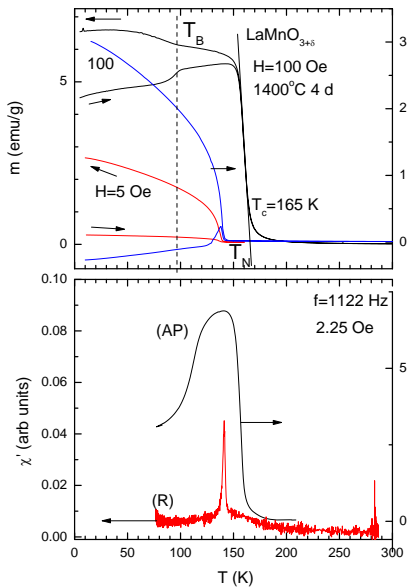


FIG. 3: (a) Temperature dependence of the dc-magnetic moment and initial ac susceptibility for the air and He atmosphere prepared  $\text{LaMnO}_3$  samples. The dc-magnetic moment was measured in ZFC and FC mode (see main text)

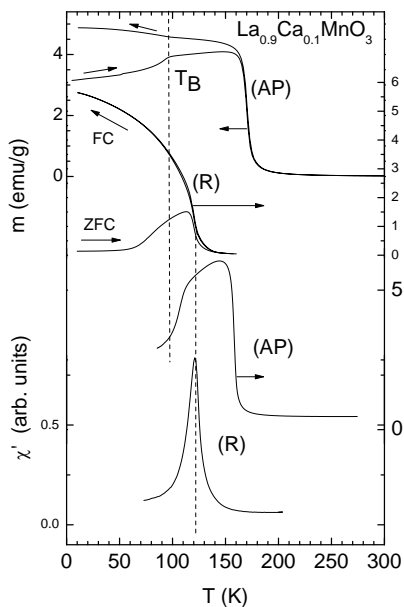


FIG. 4: (a) Temperature dependence of the dc-magnetic moment and initial ac susceptibility for the air and He atmosphere prepared  $\text{La}_{0.9}\text{Ca}_{0.1}\text{MnO}_3$  samples. The dc-magnetic moment was measured in ZFC and FC mode (see main text)

transition. However, the absence of measurable hysteresis in this regime is not in favor of a clear first order transition. On cooling under magnetic field the magnetic moment below 150 K shows a pronounced hysteresis. This thermal irreversibility of magnetization is observed below

$T_{irr}$  being a common feature of all types of magnetic systems showing magnetic hysteresis behavior. At  $T_B$  the FC branch displays a slope change so that the moment for  $T < T_B$  rises more rapidly than above  $T_B$ . The particular shape of the  $m(T)$  curve appears in all AP samples for  $0 \leq x \leq 0.2$  (see below). The lower panel of Fig. 3 shows the real part of the ac-susceptibility for both the AP and R samples. Let us firstly discuss, the data for AP sample. Below the Curie temperature,  $\chi'(T)$  increases down to the temperature where the ZFC and FC branches of the dc-moment display hysteretic behavior. Below this temperature the  $\chi'(T)$  decreases rapidly, and finally becomes nearly horizontal for  $T < T_B$ . The corresponding imaginary part (not shown) shows two peaks: one at the  $T_c$  and the other at  $T_B$ . It is interesting to note that the ac-susceptibility measurements do not show irreversible behavior.

On the other hand, the R sample shows radically different behavior. Both ac-susceptibility and the dc-magnetic moment show a lower transition temperature  $T_c = 145$  K. The ZFC and FC branches of the  $m(T)$ -curve show strong hysteretic behavior from the  $T_c$  with the ZFC branch to be far below the FC one. Isothermal magnetization measurements at  $T = 5$  K (not shown) revealed a behavior typical of a canted antiferromagnet, in agreement with neutron diffraction measurements<sup>6</sup>(the neutron diffraction data mainly show an A-type antiferromagnetic structure, because the ferromagnetic component is very small). The real part of the external susceptibility (uncorrected for demagnetizing effects)  $\chi'(T)$  displays a very narrow peak at the transition temperature.

In a case of For a canted antiferromagnet the ac-susceptibility along the ferromagnetic axis (e.g. the  $b$ -axis in our case), is expected to diverge above and below  $T_N$ . On the other hand, the ac susceptibility along the other orthogonal axes display the usual behavior for an antiferromagnetic material. In our powder sample the response is governed by the divergent part, which is larger than the antiferromagnetic one. For a canted antiferromagnet the susceptibility is expected to diverge on the interval  $\Delta T = (T_N - T_0)/T_N$  where  $\Delta T = (D/\sum_i |J_i|)^2$ ,  $T_0$  is the temperature where the susceptibility begins to diverge, and  $D$  is the anisotropy constant of crystal field type  $DS_z^2$ , or Dzyaloshinskii-Moriya interactions.<sup>23</sup> The sharp fall in  $\chi'$  below  $T_N$  can be ascribed to the onset of coercivity. As the  $x$  increases (e.g. the samples 0.05 and 0.1) the magnetic measurements for both AP and R-samples are practically similar with the  $\text{LaMnO}_3$  sample. *It is interesting to note that the width of the susceptibility peak increases with  $x$ . A fact which may be related with a softening of  $\sum_i |J_i|)^2$  with  $x$ .* In Figure 4 plotted are the dc-magnetic moment and ac-susceptibility measurements for the  $x = 0.1$  samples in order the differences with the  $x = 0.0$  sample to be emphasized. The AP-prepared sample shows exactly the same behavior as the corresponding  $x = 0.0$  sample except a slightly higher  $T_c$ . The R-sample continues to show a behavior characteristic

of a canted-antiferromagnet.

The magnetic measurements of the AP-sample  $x = 0.11$ , shows similar behavior as all the AP samples. The  $\chi'$  of the R  $x = 0.11$  sample shows two features in place of the single peak observed for  $x \leq 0.1$ . At the high temperature side of the peak of  $\chi'$  appears a clear shoulder, indicating that this sample displays two transitions. The transition located at the peak most probably is related with CAF transition of the  $x = 0.1$  sample, while the shoulder with a ferromagnetic transition. Similar behavior has been observed by Biotteau et al.<sup>6</sup> in neutron data for a single crystal with  $x = 0.1$ . Fig. 5 shows the dc magnetic moment and ac-susceptibility measurements for both AP and R  $x = 0.125$  samples. The situation in the R  $x = 0.125$  sample is more clear. Here, a ferromagnetic transition at  $T_c \approx 150$  K and a shoulder at 115 K (see arrow in Fig. 5) are observed. We attribute this anomaly to antiferromagnetic transition which in this sample occurs below  $T_c$ . The dc magnetic moment displays hysteretic behavior below  $T_{\text{irr}} \approx 140$  K, between of the ZFC and FC branches. The ZFC branch although increases non linearly with temperature, does not exhibit any other feature. At  $T = 115\text{K} \equiv T_N$  displays a maximum. The same behavior was observed in all the samples up to  $x = 0.15$  concerning the peak at  $T_c$  in the  $\chi'$  of the R samples. The shoulder now has been replaced by a broad shoulder. For  $T < 80$  K,  $\chi'$  becomes nearly horizontal. For  $x > 0.15$  the dc magnetic measurements are not essentially different in respect of the AP samples, except the lower  $T_c$  for the R samples. The step-like increment of the magnetic moment in the ZFC branches are present in both families of samples. The ac-susceptibility measurements for the R samples show an asymmetric peak at  $T_c$  and a small reduction at the temperature region where the step-like variation of the dc moment occurs. A representative example is shown in Fig. 6 for the  $x = 0.19$  sample. In the R  $x = 0.19$  sample the dc-magnetic measurements show the irreversibility at  $T_{\text{irr}} \approx 180$  K and the step at  $T_B$ . The corresponding  $\chi'(T)$  shows an asymmetric peak at  $T_{\text{irr}}$  then decreases and finally forms a shoulder at  $T_B$  before becoming horizontal.

The ac susceptibility for the samples with  $x > 0.14$  increases rapidly as  $T_c$  is approached from above, passing through a maximum at a temperature somewhat below  $T_c$ . This maximum originates from the Hopkinson effect<sup>24</sup> and not from of critical effects. The Hopkinson effect is due to the rapid increase in anisotropy with decreasing temperature below  $T_c$ , particularly when its value begins to exceed the ac field.<sup>25</sup> The application of an external static biasing field results in a rapid suppression in both amplitude and temperature of this principal maximum. The measurements under a dc field revealed a smaller secondary peak, which decreases in amplitude and moves upward in temperature as the applied field increases. This feature is a direct manifestation of critical fluctuation in a system approaching a second order paramagnetic to ferromagnetic transition and it is uniquely revealed by susceptibility measurements. This behavior

clearly appears in Fig. 7 for the  $x = 0.19$ , R sample. At this point we would like to point out that a pronounced Hopkinson peak is absent in the AP sample and in both families of samples for  $x > 0.2$ .

Our magnetic measurements for the R  $x = 0.19$  sample are in good agreement with the single crystal ones of Hong et al. ( Ref. 26). The anomaly at  $T_B$  was attributed to freezing of a cluster-glassy phase which appears below  $T_c$ . According to their neutron diffraction data this glassy phase concerns  $0.4\mu_B$  per Mn ion and has to do with charge/orbital fluctuations. For  $x > 0.2$  both families of samples show typical behavior of a low anisotropy soft ferromagnetic material.

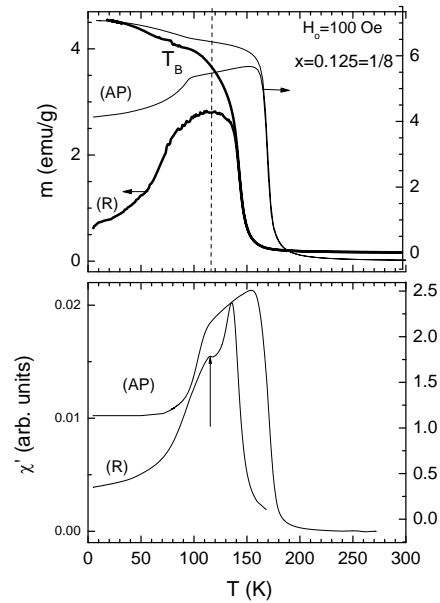


FIG. 5: Temperature dependance of the dc-magnetization (a) and initial ac-susceptibility (b) for the AP and R  $\text{La}_{0.875}\text{Ca}_{0.125}\text{MnO}_3$  samples, respectively.

## V. ELECTRICAL RESISTANCE MEASUREMENTS

Figure 8 shows representative electrical resistance measurements for R-samples in semi-logarithmic  $1/T$  plots. This kind of plots can show activation like ( $\rho = \rho_0 \exp(E_g/kT)$ , where  $E_g$  is the activation energy) variation of the resistivity. For  $T > T_c$  our resistivity curves indicate  $E_g \sim 0.1 - 0.2$  eV, increasing as  $x$  decreases (see inset of Fig. 8). The  $x = 0.23$  R-sample displays insulating behavior up to  $T_c$  where an insulator to metal transition occurs. For  $x < 0.23$  all the samples show insulating behavior. For the  $x = 0.125$  R-sample, at  $T_c$ , the resistivity can be simulated by two different activation energies above and below  $T_c$ , as it is revealed from two linear segments in the  $\log \rho$  vs.  $1/T$  plot. At  $T_c$  a reduction of the activation energy is observed. As we ap-

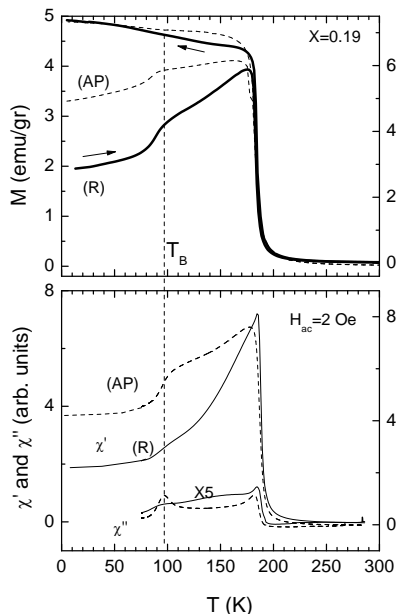


FIG. 6: Temperature dependence of the dc-magnetization (a) and initial ac-susceptibility (b) for the AP and R  $\text{La}_{0.81}\text{Ca}_{0.19}\text{MnO}_3$  samples, respectively.

proach the metal-insulator transition (near  $x = 0.23$ ) the change of the activation energy occurs in a step like fashion, while the resistivity curve below  $T_c$  diverges from the activation like behavior so that the  $E_g$  effectively diminishes as temperature decreases. The corresponding measurements for the AP-samples also show insulating behavior with a slope change at  $T_c$  but the metallic behavior now occurs for lower  $x = 0.2$ . We must note that other researches have interpreted the step-like change of the  $\rho$  right below  $T_c$  in the  $\rho(T)$  curve for the  $x = 0.22$  R-sample, as an insulator to metal behavior, which subsequently is transformed to a metal to insulator behavior. To our opinion this is a relative broad change of the electronic structure at  $T_c$ , producing this abrupt change of  $E_g$ . In other words, the ferromagnetic insulating regime is characterized by ferromagnetic insulated ground state. The magnetic ordering seems that abruptly renormalizes the electronic gap near the center ( $x = 0.18$ ) of the ferromagnetic insulating regime. As the low boundary  $x = 0.125$  is approached, this type of renormalization becomes more smooth, while at the upper boundary the change is more intense, since, there, we have complete change of the electronic structure (metallic ground state).

## VI. PHASE DIAGRAM

Based on the magnetic measurements, the magnetic phase diagram for both families of  $\text{La}_{1-x}\text{Ca}_x\text{MnO}_3$  samples are determined and plotted in Fig. 9. The AP sam-

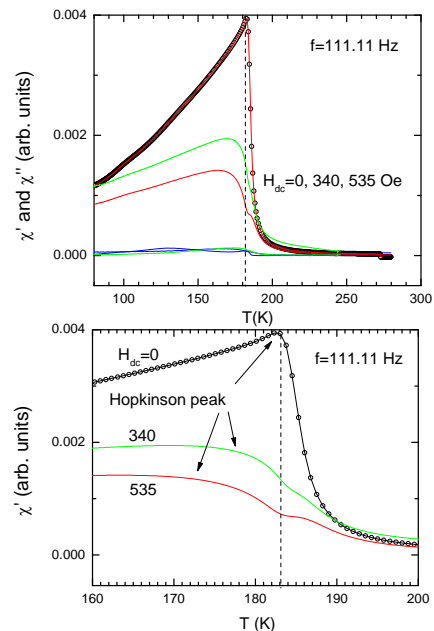


FIG. 7: Temperature variation of the linear fundamental ac-susceptibility for various dc fields of the  $x = 0.19$  R sample.

ples display a ferromagnetic transition at  $T_c(x)$ , which increases with  $x$  (see Fig. 9(a)). In this figure plotted also are the onset points  $T_B(x)$ , where the step increment of the magnetic moment is observed. The temperature where this transition occurs is nearly independent of  $x$ . Although this transition persists and for  $x > 0.2$  the height of the magnetic moment "jump" diminishes significantly there. The physical origin of the  $T_B$  is the subject of several recent publications but its complete elucidation has not yet been achieved. Fig. 9(b) shows the phase diagram of the R samples, which is radically different in comparison with it of the AP samples, especially for  $x < 0.15$ . Our results for the R samples are in nice agreement with those of Ref. 6,27, where stoichiometric single crystals have been studied. For  $0 \leq x < 0.125$  the R samples undergo a transition from a paramagnetic to a canted antiferromagnetic state at  $T_N$ . The  $x = 0$  sample is an  $A_x$ -type antiferromagnet with a small ferromagnetic component along the  $b$ -axis ( $Pnma$  notation). As  $x$  increases the ferromagnetic component of the canted magnetic structure increases in expense of the antiferromagnetic one. For  $x > 0.08$  it is clear that antiferromagnetic and ferromagnetic transitions occur at different temperatures ( $T_N < T_c$ ). For  $0.125 \leq x \leq 0.2$  according to the magnetic saturation measurements all the samples show ferromagnetic behavior. However, the real character of the zero field ground state is not clear. The dc magnetic and ac-susceptibility measurements show a rather complex behavior. Let us describe the possible physical origin of the special features observed in magnetic measurements for R samples. Fig. 10 clearly shows this behavior. We have plotted the  $\chi'(T)$  for all the R-



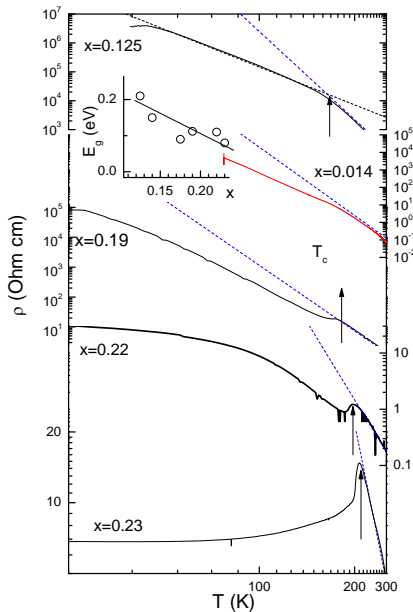


FIG. 8: Temperature variation of the electrical resistivity of the R-samples in  $\log -1/T$  plots. The straight dashed lines are plots of the equation ( $\rho = \rho_0 \exp(E_g/kT)$ ). The estimated  $E_g(x)$  is shown at the inset.

samples. The first transition appears as peak and has to do with ferromagnetic interactions of the canted structure for  $0.125 < x \leq 0.15$ . Subsequently, instead the peak decrease itself considerably as in the CAF structure after a wide shoulder it remains temperature independent down to zero temperature. At the same time the dc-magnetic moment presents smaller difference between ZFC and FC branches in comparison to the CAF structure. All these observations imply that we have a behavior where the mechanism, which is responsible for the CAF structure weakens more and more as  $x$  goes away from  $x = 0.125$ . It seems that the anomaly related with  $T_N$  for  $x < 0.125$  is transformed to the anomaly at  $T_B$ .

Having attributed the sharp peak right below  $T_c$  in the middle of the insulating ferromagnetic regime to the Hopkinson effect (rapid increase of the magnetic anisotropy) we can conclude that in the ferromagnetic insulating regime of the R-samples is related with magnetic anisotropy increment. This increment reduces as the metallic boundary is approached. On the other hand, this anisotropy increases on approaching the canting antiferromagnetic boundary. This significant conclusion may have to do with the idea of some kind of orbital ordering<sup>13,28</sup> or orbital domains<sup>29</sup> occurring in the ferromagnetic-insulating regime. A new kind of orbital ordering below  $T_c$ , for a sample with nominal composition  $\text{La}_{0.85}\text{Ca}_{0.15}\text{MnO}_3$  has been proposed in Ref. 30. At  $T = 2$  K the high resolution neutron diffraction pattern is compatible with a monoclinic distortion, described from

the space group  $P2_1/c$ . In this structural model there are two nonequivalent  $\text{MnO}_2$  layers alternating along the  $a$ -axis leading to a specific pattern of Mn-O distances, implying an unconventional orbital ordering type. This model may be relevant with the ferromagnetic insulating state, where a specific orbital ordering was proposed. However, the metallic resistivity variation of the particular sample, takes in question the generalization of this model in describing the FI phase.

We must note that, as the magnetic measurements show, in the metallic regime ( $x \geq 0.23$ ) no Hopkinson peak is present, a fact which tells us that here the magnetic anisotropy goes to zero smoothly at  $T_c$ . Concerning the AP-samples, they do not show the Hopkinson peak also at  $T_c$ , implying that the mechanism which is responsible does not operate in this case. Let us turn now on the feature at the  $T_B$ . This feature is present in all the AP-samples while it is less pronounced in the R-samples. It is reasonable that in the R-samples the anomaly in the magnetic measurements at low temperatures may be related with some kind of antiferromagnetic interaction as the CAF boundary is approached. These antiferromagnetic interactions may produce some kind of glassiness with diminished weight as the metallic boundary is approached. The detailed microscopic origin of the anomaly at  $T_B$  is not clear.

In some works the feature at  $T_B$  has been attributed to the sudden change of the domain wall dynamic due to the domain wall pinning effects.<sup>31</sup> As also observed, small frequency dependence of the peak in the  $\chi''$ , at temperature where the step occurs, is not an indication of spin glass behavior. Many magnetically ordered systems exhibit frequency dependence without this to mean spin-glass behavior. This dependence has been attributed to the freezing out of domain wall motion which is a consequence of the rearrangements of electron states within the domain wall. The low field ZFC magnetization follows the changes of coercivity which is directly related with the magnetocrystalline anisotropy. If this scenario is correct then which is the origin of this sudden change in the magnetocrystalline anisotropy? Laiho et al.<sup>32</sup> using air atmosphere prepared samples based mainly on frequency dependence of  $\chi'$  at the region where the step was observed they attributed this feature to a reentrant spin glass phase. It is well known that the compound with  $x = 0.5$  undergoes a first order charge/orbital ordering antiferromagnetic transition below the Curie temperature. This transition has as consequence the appearance of a diminish of the magnetization in both FC and ZFC magnetization branches. Something which is not observed in our measurements, where ZFC and FC branches follow opposite direction for  $T < T_B$ .

The physics of the AP samples near  $x = 0$  may be related with the results of Algarabel et al. (Ref. 33). In this study, based on small angle neutron scattering data, was suggested that the ferromagnetic phase (for  $T < T_c$ ) comprises from clusters increasing in size as the temperature decreases reaching the value of 3-3.5 nm at low

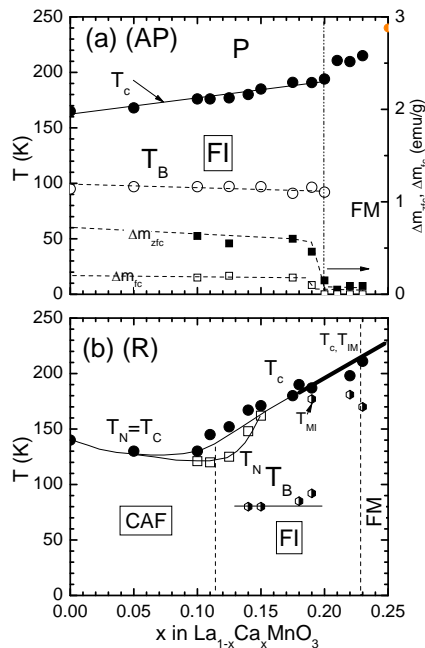


FIG. 9: (a) Phase diagram for the air atmosphere prepared  $\text{La}_{1-x}\text{Ca}_x\text{MnO}_3$  samples. The solid circles denote the paramagnetic ferromagnetic transition. The open circles corresponds to the onset temperature  $T_B$  of the jump in the ZFC dc-magnetization curves. The open and closed squares shows the temperature variation of the magnetization jump-size during field and zero-field cooling modes, respectively. (b) Phase diagram for R (He atmosphere annealed)  $\text{La}_{1-x}\text{Ca}_x\text{MnO}_3$  samples. The solid circles denote the transition from the paramagnetic to canted antiferromagnetic or ferromagnetic. The semi-filled circles for  $x > 0.125$  correspond to the onset temperature  $T_B$  of the jump in the ZFC dc-magnetization measurements.

temperature. It is plausible that the non-stoichiometric samples as the AP ones may consist from regions rich in holes (then ferromagnetic) and poor in holes (with glass behavior).

The magnetic measurements of Ref. 34,35 practically coincide with ours for the R-sample with nominal composition  $x = 0.15$ . It is most probable that in the single crystal the stoichiometry is slightly lower from the nominal one. In the particular crystal they observed a ferromagnetic to paramagnetic and metal-insulator transition at  $T_c \approx 180$  K, a ferromagnetic-insulator transition at  $T_{\text{FI}} \approx 150$  K and a magnetic anomaly at  $T_B \approx 95$  K, which is related with a level off of the resistivity.

Finally, it is interesting to compare the present magnetic measurements with those of the  $\text{La}_{1-x}\text{Sr}_x\text{MnO}_3$  at FI regime occurring at  $x = 0.125$ . This compound firstly exhibits a cooperative Jahn-Teller first-order transition at  $T_{\text{JT}} \approx 270$  K, secondly, a transition towards a ferromagnetic and metallic state, at  $T_c = 181$  K and then, a magneto-structural first-order transition into a ferro-

magnetic insulating state, at  $T_B = 159$  K. The transition at  $T_B = 159$  K is characterized by a jump in the

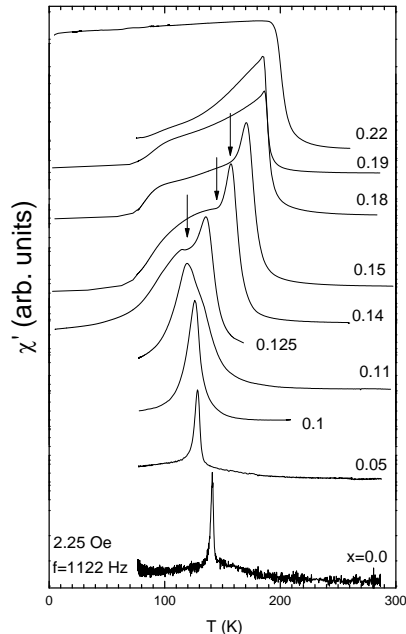


FIG. 10: Temperature dependence of the  $\chi'$  for the R  $\text{La}_{1-x}\text{Ca}_x\text{MnO}_3$  samples ( $0 \leq x \leq 0.22$ ), respectively.

magnetization<sup>17,19,36,37,38</sup>, a typical for first-order transition delta function-like variation of the specific heat, appearance superstructure peaks, significant decreasing of the orthorhombicity and the three characteristic Mn-O distances become very close to each other. In addition Moussa et al.<sup>39</sup> have found a splitting of the spin waves, an opening of a gap at  $\mathbf{q} = (0, 0, 1/2)$  ( $Pnmb$  notation) and a locking of the spin wave energy on the energy values of phonons. All the above features occurring at  $T < T_B$ , are indicative for a first order transition, most probably, related with a new orbital order.<sup>17</sup>

Summarizing, in this work we have performed a systematic study of  $\text{La}_{1-x}\text{Ca}_x\text{MnO}_3$  ( $0 \leq x \leq 0.2$ ) with aim at advancing the knowledge of the underlying mechanisms which influence their structure and magnetic properties. The results of the present work clearly demonstrate that the physical properties of the low doped  $\text{La}_{1-x}\text{Ca}_x\text{MnO}_3$  compound depend on the oxygen partial pressure during the preparation influencing the  $\text{Mn}^{+4}$  content. In order stoichiometric samples to be prepared a low oxygen partial pressure is needed. The samples prepared in atmospheric conditions for  $x < 0.16$  are cations deficient and in a such a way so that the amount of the  $\text{Mn}^{4+}$  to remain constant regardless of  $x$ . The ferromagnetic insulating regime near the  $x = 0.2$  boundary for both families of samples is not homogeneous.



- 
- <sup>1</sup> E. O. Wollan and W. C. Koehler, Phys. Rev. **100**, 545 (1955).
- <sup>2</sup> J. B. Goodenough, Phys. Rev. **100**, 564 (1955).
- <sup>3</sup> P. Schiffer, A. P. Ramirez, W. Bao and S. -W. Cheong, Phys. Rev. Lett. **75**, 3336 (1995).
- <sup>4</sup> A. P. Ramirez, P. Schiffer, S. -W. Cheong, C. H. Chen, W. Bao, T. T. Palstra, P. L. Gammel, D. J. Bishop and B. Zegarski, Phys. Rev. Lett. **76**, 3188 (1996).
- <sup>5</sup> T. Okuda, Y. Tomioka, A. Asamitsu, and Y. Tokura, Phys. Rev. B **61**, 8009 (2000).
- <sup>6</sup> G. Biotteau, M. Hennion, F. Moussa, J. Rodriguez-Carvajal, L. Pinsard, A. Revcolevschi, Y. M. Mukovskii, and D. Shulyatev, Phys. Rev. B **64**, 104421 (2001).
- <sup>7</sup> M. Pissas and G. Kallias, Phys. Rev. B **68**, 134414 (2003).
- <sup>8</sup> E. Dagotto, T. Hotta, and A. Moreo, Phys. Rep. **344**, 1 (2001).
- <sup>9</sup> J. Kanamori, J. Appl. Phys. **31**, 14S (1960).
- <sup>10</sup> J. Rodriguez-Carvajal, M. Hennion, F. Moussa, A.H. Moudden, L. Pinsard, and A. Revcolevschi, Phys. Rev. B **57**, R3189 (1998); Y. Murakami, J.P. Hill, D. Gibbs, M. Blume, I. Koyama, M. Tanaka, H. Kawata, T. Arima, Y. Tokura, K. Hirota, and Y. Endoh, Phys. Rev. Lett. **81**, 582 (1998); M. Imada, A. Fujimori, and Y. Tokura, Rev. Mod. Phys. **70**, 1039 (1998).
- <sup>11</sup> K. I. Kugel' and D. I. Khomskii, Sov. Phys. Usp. **25**, 231 (1982).
- <sup>12</sup> F. Moussa, M. Hennion, G. Biotteau, J. Rodriguez-Carvajal, L. Pinsard and A. Revcolevschi, Phys. Rev. **60**, 12299 (1999).
- <sup>13</sup> Bas B. Van Aken, Oana D. Jurchescu, Auke Meetsma, Y. Tomioka, Y. Tokura and Thomas T. M. Palstra, Phys. Rev. Lett. **90**, 066403 (2003).
- <sup>14</sup> J. W. Lynn, R. W. Erwin, J. A. Borchers, Q. Huang, A. Santoro, J.-L. Peng, and Z. Y. Li, Phys. Rev. Lett. **76**, 4046 (1996).
- <sup>15</sup> Pengcheng Dai, J. A. Fernandez-Baca, N. Wakabayashi, E. W. Plummer, Y. Tomioka, Y. Tokura, Phys. Rev. Lett. **85**, 2553 (2000).
- <sup>16</sup> J. A. Fernandez-Baca, P. Dai, H. Y. Hwang, C. Kloc, and S.-W. Cheong, Phys. Rev. Lett. **80**, 4012 (1998).
- <sup>17</sup> Y. Endoh, K. Hirota, S. Ishihara, S. Okamoto, Y. Murakami, A. Nishizawa, T. Fukuda, H. Kimura, H. Nojiri, K. Kaneko, and S. Maekawa, Phys. Rev. Lett. **82**, 4328 (1999).
- <sup>18</sup> Y. Yamada, J. Suzuki, K. Oikawa, J. A. Fernandez-Baca, Phys. Rev. B **62**, 11600 (2000).
- <sup>19</sup> B. Dabrowski, R. Dybziński, Z. Bukowski, and O. Chmaissem, J. Solid State. Chem. **146**, 448 (1999).
- <sup>20</sup> Q. Huang, A. Santoro, J. W. Lynn, R. W. Erwin, J. A. Borchers, J. L. Peng and R. L. Greene, Phys. Rev. B **55**, 14987 (1997).
- <sup>21</sup> Q. Huang, A. Santoro, J. W. Lynn, R. W. Erwin, J. A. Borchers, J. L. Peng, K. Ghosh and R. L. Greene, Phys. Rev. B **58**, 2684 (1998).
- <sup>22</sup> J. Rodriguez-Carvajal, Physica B **192**, 55 (1992).
- <sup>23</sup> T. Moriya, *Magnetism I* (3), edited by Rado and Suhl (Academic Press, New York, 1963).
- <sup>24</sup> G. Williams, in *Magnetic Susceptibility of Superconductors and Other Spin Systems*, edited by R. A. Hein *et al.* (Plenum, New York, 1991). p475; J. H. Zhao, X. Z. Zhou, A. Peles, S. H. e, H. P. Kunkel, and Gwyn Williams, Phys. Rev. B **59**, 8391 (1999).
- <sup>25</sup> S. Chikazumi, in *Physics of Magnetism* (Wiley, New York 1964).
- <sup>26</sup> C. S. Hong, E. O. Chi, W. S. Kim, N. H. Hur and Y. N. Choi, J. of the Phys. Soc. of Japan, **71**, 1583 (2002).
- <sup>27</sup> P. Mandal and B. Ghosh, Phys. Rev. B **68**, 014422 (2003).
- <sup>28</sup> M. Hennion, F. Moussa, F. Wang, J. Rodríguez-Carvajal, Y. M. Mukovskii, and D. Shulyatev, cond-mat/0112159 (2001).
- <sup>29</sup> G. Papavassiliou, M. Pissas, M. Belesi, M. Fardis, J. Dolinsek, C. Dimitropoulos, and J. P. Ansermet, Phys. Rev. Lett. **91**, 147205 (2003).
- <sup>30</sup> M. V. Lobanov, A. M. Balagurov, V. Ju. Pomjakushin, P. Fischer, M. Gutmann, A. M. Abakumov, O. G. D'yachenko, E. V. Antipov, O. I. Lebedev and G. Van Tendeloo, Phys. Rev. B, **61**, 8941 (2000).
- <sup>31</sup> P.A. Joy, S. K. Date, J. of Magn. Magn. Mat. **220**, 106 (2000).
- <sup>32</sup> R. Laiho, et al. Phys. Rev. B **63**, 094405 (2001)
- <sup>33</sup> P. A. Algarabel, J. M. De Teresa, J. Blasco, M. R. Ibarra, Cz. Kapusta, M. Sikora, D. Zajac, P. C. Riedi, C. Ritter, Phys. Rev. B **67**, 134402 (2003).
- <sup>34</sup> V. Markovich, I. Fita, R. Puzniak, M. I. Tsindlekht, A. Wisniewski, and G. Gorodetsky, Phys. Rev. B **66**, 094409 (2002).
- <sup>35</sup> V. Markovich, E. Rozenberg, A. I. Shames, and G. Gorodetsky, I. Fita Donetsk, K. Suzuki, R. Puzniak, D. A. Shulyatev and Ya. M. Mukovskii, Phys. Rev. B **65**, 144402 (2002).
- <sup>36</sup> S. Uhlenbruck, R. Teipen, R. Klingeler, B. Bchner, O. Friedt, M. Hcker, H. Kierspel, T. Niemöller, L. Pinsard, A. Revcolevschi, and R. Gross, Phys. Rev. Lett. **82**, 185 (1999).
- <sup>37</sup> P. Wagner, I. Gordon, S. Mangin, V. V. Moshchalkov, Y. Bruynseraede, L. Pinsard, A. Revcolevschi, Phys. Rev. B **61**, 529 (2000).
- <sup>38</sup> G.-L. Liu, J.-S. Zhou, J. B. Goodenough, Phys. Rev. B, **64**, 144414, (2001).
- <sup>39</sup> F. Moussa, M. Hennion, F. Wang, P. Kober, J. Rodriguez-Carvajal, P. Reutler, L. Pinsard, and A. Revcolevschi, Phys. Rev. B **67**, 214430 (2003).